Tree log identification based on digital cross-section images of log ends using fingerprint and iris recognition methods

Rudolf Schraml Heinz Hofbauer Andreas Uhl
University of Salzburg
Jakob Haringer Str. 2, 5020 Salzburg
{rschraml,hhofbaue,uhl}@cosy.sbg.ac.at

Abstract

Tree log biometrics is an approach to establish log traceability from forest to further processing companies. This work assesses if algorithms developed in the context of fingerprint and iris recognition can be transferred to log identification by means of cross-section images of log ends. Based on a testset built up on 155 tree logs the identification performances for a set of configurations and in addition the impacts of two enhancement procedures are assessed.

Results show, that fingerprint and iris recognition based approaches are suited for log identification by achieving 100% detection rate for the best configurations. In assessing the performance for a large set of tree logs this work provides substantial conclusions for the further development of log biometrics.

1. Introduction

Commonly the term biometrics stands for the study of behavioural or physiological characteristics to identify living people. But the theoretical background and the concepts of human biometrics have been carried over to the recognition of plants, vegetables, animals, industrial products and most relevant for this study to the recognition of tree logs or boards [19]. This study deals with concepts of fingerprint and iris recognition and explores their applicability to the identification of tree logs using cross-section images (CS-Images) of log ends.

In order to close the traceability gap between the forest site and the further processing companies tree log identification is an economic requirement to map the ownership of each log. Additionally, social aspects have become more important and sustainability certificates like Pan European Forest Certification (PEFC) and Forest Stewardship Council (FSC) are a must have for all end-sellers. Finally, traceability is legally bound by the European Timber Regulation (EUTR) to prohibit illegal logging in the EU [4].

State-of-the art traceability approaches rely on physically marking each log and in the past decade huge efforts were taken to push the development of new traceability approaches. For example, the final report of the Indisputable Key Project [18] promotes the usage of Radio Frequency Identification transponders to establish log traceability.

First investigations on the hypothesis that logs are separate entities on the basis of biometric log characteristics were carried out in the works of [2, 3, 5]. 2D and 3D scanners were used to extract geometric wood properties and the experiments showed low recognition rates. Furthermore, the utilized capturing devices are not applicable for industrial usage at forest site.

On account of the fact, that log end faces show features in terms of annual rings, pith position, shape and dimension it is assumed that CS-Images of log ends can be used as biometric characteristic to set-up a biometric system. A first work on log biometrics using CS-Images was presented by [1] as an effort to curb poaching of trees. For this purpose, pseudo Zernike moments are computed for CS-Images captured from poached tree stumps and first results were presented for a small testset. The achieved results were quite good but the extracted features more or less rely on the cutting pattern and the shape of the CS.

By superficially comparing annual ring patterns of log ends to human fingerprints one perceives their similarity. Based on this observation, [15] investigated temporal and longitudinal variances of CS-Images of a single tree log. The authors adopted the FingerCode approach [7] to compute and compare templates from CS-Images. Furthermore, in [14] the impact of different real world CS variation types on the robustness of biometric log recognition is assessed. Although the authors draw first conclusions on the identification performance, the utilized testset is too small and the results are not convincing.

In considering the identification performance for 150 different tree logs this work demonstrates that a biometric system using log end images is suited for log tracking. Additionally to the fingerprint-based approach utilized

in [15, 14], this work evaluates the applicability of well-known iris recognition approaches. Furthermore, it is not clear to which extent the enhancement procedure utilized in [15, 14] influences the verification and identification performance. For this purpose, all approaches are evaluated with and without enhancement. Results show, that enhancement basically is beneficial to overcome issues caused by CS variations but it also introduces an error which deteriorates the overall performance.

Section 2 introduces the computation and matching of log templates using approaches from fingerprint and iris recognition. Subsequently, the experimental evaluation is presented in Section 3 followed by the conclusions in Section 4.

2. CS-Code Computation and Matching

An exemplary enrolment and identification scheme for log biometrics is depicted in Fig. 1. Enrolment of a tree log is performed in the forest. After a tree log is cut and processed by a harvester the log end is captured by a digital camera mounted on the harvester head. Templates of logs which are computed by means of CS-Images are denoted as CS-Codes. For enrolment the computed CS-Code is stored in the database. Identification can be performed at

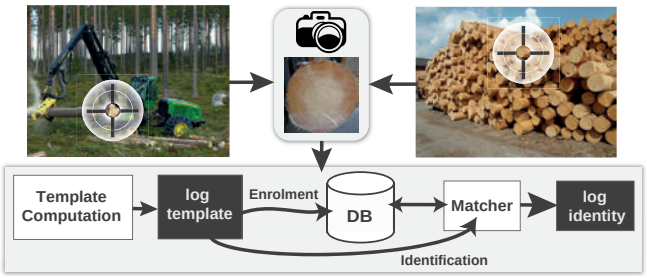

Figure 1: Exemplary enrolment and identification schemes

each stage of the log processing chain where an appropriate capturing device is available. Typically, identification is required when a log is delivered to a sawmill. Independent of the template computation approach procedure the CS-Image is registered and enhanced preliminary. The fingerprint and iris-based CS-Code computation schemes are depicted in Fig. 2.

2.1. CS Registration and Enhancement

For registration the pith position and CS boundary have to be determined in advance. Automated approaches for pith estimation and CS segmentation were presented in [16, 11] and [17], respectively. The CS-Image is rotated around the pith position, cropped to the CS boundary box and scaled to 512 pixels in width. Rotation is performed to generate rotated versions of the input image or to align the CS to a unique rotational position.

The registered CS-Image is then utilized for the enhancement procedure. Commonly, the annual ring pattern is disturbed due to cutting and there arise different types of intraclass CS variations in real world identification scenarios [14]. The purpose of enhancement is to strengthen the annual ring pattern contrast and to compensate CS variations. Similarly to fingerprint enhancement [6], three consecutive stages are performed: Local orientation estimation, local frequency estimation and local adaptive filtering. Initially, the CS-Image is subdivided into half-overlapping blocks to reduce boundary effects caused by local filtering. On the basis of registered CS-Images which are scaled to 512 pixels in width, 32×32 pixels blocks are a good choice in terms of timing performance and capturing local annual ring pattern information.

In the first stage, the local orientation of each block is determined based on peak estimation in the Fourier Spectrum (see [16]). Next, the local orientation field is low-pass filtered with a Gaussian to correct wrong orientation estimates. Based on the orientation estimates of each block the corresponding dominant frequency in the Fourier Spectrum is determined. Therefore, the Fourier Spectrum of each block is subdivided into sub-bands and sectors and the dominating frequency is defined as the sector sub-band which shows the maximum integral of its magnitudes. If this sector sub-band does not correspond to the block orientation it is neglected and the local frequency is interpolated using a Gaussian. Finally, the Fourier Spectrum of each block is filtered with a Log-Gabor which is tuned to the block orientation and frequency. As in [15] a bandwidth of three times the variance of the Fourier Spectrum and as spread value the blocksize/4 is utilized. After filtering, the filtered spectra are inverse transformed and utilized as new block values.

In this work additionally a variant of this procedure is evaluated which differs in the local orientation estimation procedure. Initially, local orientations are computed for each block as described above. Subsequently, the pith position is used to detect wrong orientation estimates in case the angular distance between the block origin/pith position and the local orientation estimate exceeds a threshold. Thereby, the threshold for a each block is specified by $t = \lambda * log(\text{pith distance})$, where λ is an arbitrary value and the pith distance is the distance between the block origin and the pith. Thus, the threshold increases with an increasing pith distance which takes into account that annual rings close to pith are more circular. For each local orientation estimate which exceeds this threshold the estimate is replaced by the direction to the pith position. All further steps are performed equally as for the first approach.

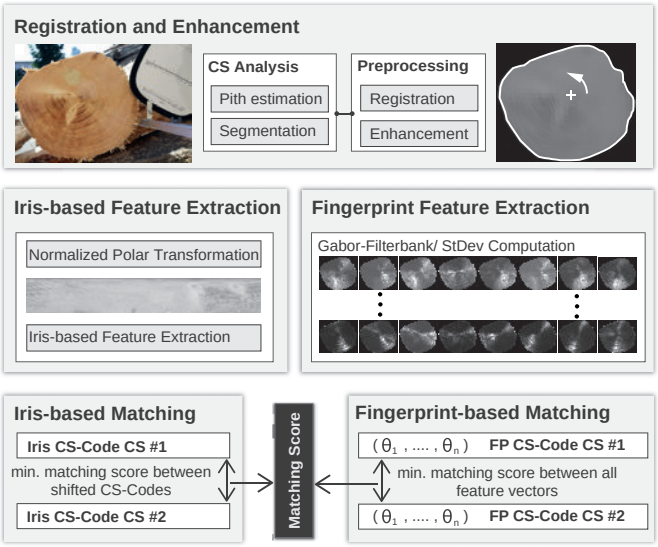

Figure 2: Fingerprint and iris based template computation and matching schemes

2.2. Fingerprint-based CS-Codes

Equal as in [15, 14] the FingerCode approach is adopted to compute and compare CS-Codes from CS-Images. With intent to capture different annual ring pattern frequencies the utilized Gabor filterbank is built up on six different filters and for each filter eight rotated versions are created. CS-Code computation is performed in three stages: First, the registered and enhanced CS-Image is filtered with each filter in the filterbank. The filtered images are further subdivided into blocks (e.g. 16×16 pixels). For all blocks of each filtered image, the grey value standard deviations are computed and stored into a matrix. Values of blocks which are not within the CS border are assigned with a marker value (e.g. -1) which is relevant for CS-Code matching. All matrices are stored as a one-dimensional vector.

Rotational variances are compensated by repeatedly computing features for rotated versions of the input CS-Image. Compared to fingerprints, the rotational misalignment range of a CS-Image is not restricted to a certain range. Therefore, rotational pre-alignment can be performed in the registration and enhancement stage. All feature vectors computed for different rotations $(\Theta_1, \ldots, \Theta_n)$ compose the CS-Code of a CS-Image.

Matching procedures Matching between two CS-Images is performed by computing the minimum matching score (MS) between all feature vectors $(\Theta_1, ..., \Theta_n)$ of the CS-Codes from both CS-Images. Three different matching procedures are evaluated to investigate the impact of including shape information. The MS is computed by:

$$MS(CS_1, CS_2) = \frac{1}{M} \sum_{i=0}^{N} D(CS_1(i), CS_2(i)) \quad (1)$$

where CS_1, CS_2 are two feature vectors of the CS-Codes which are compared, i specifies the index of the feature value in both vectors and MCS_1, MCS_2 are masks which allow to differentiate between background and CS.

The first matching procedure MS_{AP} uses a distance function which just uses feature value pairs which are in the intersection of both CSs . For normalization, M is defined by the amount of considered feature value pairs: $M = |MCS_1 \cap MCS_2|$. Thus, this procedure relies on the discriminative power of the annual ring pattern.

$$D_{AP} = \begin{cases} |CS_1(i) - CS_2(i)| & \text{if } i \in MCS_1 \cap MCS_2 \\ 0 & \text{otherwise} \end{cases} \quad (2)$$

For the second procedure $MS_{AP\&S}$ the distance function $D_{AP\&S}$ includes a penalty value $P_{AP\&S}$. The penalty is added to all feature value pairs which are in the symmetric difference of the CS masks and for normalization $M = |MCS_1 \cup MCS_2| + |MCS_1 \triangle MCS_2|$ is used. Hence, the MS increases for differently shaped CSs. $P_{AP\&S}$ is defined by the mean value of the feature value distributions of both feature vectors.

$$D_{AP\&S} = \begin{cases} |CS_1(i) - CS_2(i)| + P_{AP\&S} & \text{if } i \in MCS_1 \triangle MCS_2 \\ |CS_1(i) - CS_2(i)| & \text{if } i \in MCS_1 \cap MCS_2 \\ 0 & \text{otherwise} \end{cases} \quad (3)$$

Finally, the third procedure uses score level fusion of the MS_{AP} score and the False Negative Rate (F) which is computed for (MCS_1, MCS_2). F is defined as the ratio between the symmetric difference of the two masks and total amount of pixels in the smaller mask. For score level fusion MS_{AP} and F are normalized using different factors σ_{AP}, σ_F so that they become equally weighted in the score level fusion.

$$\mathrm{F} = \frac{MCS_1 \triangle MCS_2}{\min(|MCS_1|, |MCS_2|)}, \; MS_{AP,F} = MS_{AP} \cdot \sigma_{AP} + F \cdot \sigma_F \quad (4)$$

2.3. Iris-based CS-Codes

The pith of a cross-section is a unique feature which can be used as reference point. In combination with the CS border it is used to polar transform CS-Images. In this work polar transformed CS-Images are treated like polar iris images and it is evaluated if iris feature extractors and comparators are applicable for log biometrics.

For this purpose, the registered and enhanced CS-Image is transformed by using bi-cubic interpolation. For normalization each pixel in the polar image is stretched according to the max. pith to border radius. Two different formats for the polar-transformation are evaluated. The first is equal to

the usual format demanded by many iris feature extractors: 512×64 pixels. Compared to the size of the iris, CSs are larger and the transformation is not restricted to an annular shaped ring. Thus, a second format with 512×512 pixels is evaluated. The polar transformation scheme is depicted in Fig. 3. For iris recognition based CS-Code computation and template matching the USIT package [13] is utilized (see Section 3).

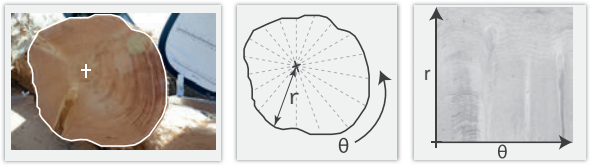

Figure 3: CS-Image polar transformation scheme

3. Experiments

In the experiments the verification and identification performances for different configurations are assessed. Introductory, the testset is outlined and the experimental setup for the utilized configurations is described (see Section 3.1). Finally, the results are presented and discussed in Section 3.2.

Testset Two testsets (TS_1 and TS_2) form the basis for the experimental evaluation. For TS_1 50 different tree logs were captured four times with and without flash. Additionally, the ends of eight logs were cross-cut and captured once again, with and without flash. In TS_2 105 logs were captured three times without flash. For each CS-Image the pith position and the CS border were determined manually and are utilized for the experiments.

Figure 4: Testset One (TS_1): Each row shows four CS-Images of a single log. The first two CS-Images illustrate the difference of capturing the log end with and without flash. The latter two images are taken after the log end was cross-cut, with and without flash.

3.1. Experimental Setup

For all CS-Images of the testsets CS-Codes and MSs were computed for different configurations and enhancement procedures. Subsequently, the setup for the enhancement procedures and the different CS-Code computation approaches are outlined.

Figure 5: Testset Two (TS_2): CS-Images from 8 logs

Enhancement The first procedure, entitled as ENH_1, is equal to the procedure suggested in [15]. As described in Section 2.1 the second just differs in the local orientation estimation procedure and is entitled as ENH_2. For comparison, all configurations are additionally evaluated without enhancement ENH_{no}.

Fingerprint (FP) configurations Rotational variances are compensated by computing feature vectors for rotations in the range from $-15°$ to $15°$. The CS-Codes are computed using 16×16 non-overlapping blocks and the Gabor filterbank is build up on six different filters tuned to 8 directions: $G(\lambda, \theta, \sigma, \gamma) = G(\lambda, \sigma) = ((1.5, 2), (2.5, 2), (3.5, 3), (4.5, 3), (5.5, 3), (6.5, 3)), \theta = \{0, 22.5, ..., 135, 157.5\}, \gamma = 0.7$

Iris configurations Different configurations based on the feature extractors and comparators provided by the USIT package [13] are utilized. In addition, two different formats for the CS-Image polar-transformation are evaluated: 512×64 and 512×512 pixels. In case of 512×64 pixels we utilize the following feature extractors: lg [10], ko [8], cr [12] and qsw [9]. Except for ko which uses koc as comparator all MSs are computed using the Hamming distance (hd).

For 512×512 pixels polar CS-Images the lg algorithm was extended to textures bigger than the 512×64 in accord with the original algorithm by defining the region of interest (ROI) through a number of rows r with a height h_r. Like the original, a row is condensed into a 1-D signal which is run through the Gabor filtering process. Since it is not clear which configuration of r and h_r is best we choose to use a variance of combinations, including combinations where the ROI does not span the whole texture. However, unlike the iris biometry case which excludes the outer iris boundary, which frequently exhibits occlusions by cilia, we choose to exclude the inner texture, which essentially stretches a low number of pixels to the texture width, thus providing nearly no usable information. Note that the size of the feature vector is dependent on h_r. Furthermore the algorithm by Ko et al. was simply adopted by allowing bigger textures without adapting the cell-size which is averaged. Note that as a result the length of the feature vector increases with the size of the texture. Rotational variances are compensated by shifting the CS-Codes in a range be-

tween -7 to 7 feature vector positions.

3.2. Results and Discussion

The experimental evaluation is performed in two stages. First, we evaluate the verification and identification performance for all configurations. Based on the EERs and Rank 1 recognition rates conclusions on the general applicability of the FP and iris approaches and the impact of enhancement are presented. Second, a closer examination on the intra- and interclass score distribution (SD) subsets points out how the enhancement and CS variations affect the intra- & interclass separability and thus the biometric system performance.

3.2.1 Verification Performance Evaluation

The EERs for all configurations computed for TS_1 and TS_2 are depicted in Table 1. Most important for this work, most of the EERs are quite low and show a high degree of separability between the intra- and interclass SD for a large set of tree logs.

	Configuration	Enh_{NO}	Enh_1	Enh_2
FP	MS_{AP}	15.7	1.7	0.9
	$MS_{AP\&S}$	1.85	0.74	0.68
	$MS_{AP,F}$	1.53	0.37	0.17
IRIS 512x512	lg, hd(16/32)	0.21	0.68	0.82
	lg, hd(50/10)	0.16	0.72	0.32
	lg, hd(64/08)	0.16	0.76	0.51
	ko, koc	2.73	4.88	4.24
IRIS 512x64	cr, hd	5.27	3.41	4.97
	lg, hd	1.34	3.64	5.42
	qsw, hd	3.44	5.73	8.33
	ko, koc	4.95	8.09	7.35

Table 1: EERs [%] for the FP and iris configurations

Equal as in [14] the EERs of the FP configurations show that shape information improves the verification performance. Except MS_{AP}, all other configurations include shape information in some way, e.g. the polar transformation relies on the CS boundary. Basically, the results for MS_{AP} show the discriminative power of the annual ring pattern solely and it is very amazing that MS_{AP} and ENH_2 achieves an EER of 0.9%. As expected, the utilized enhancement procedures improve the EERs of all FP configurations. Furthermore, the results of the FP configurations show that ENH_2 leads to better EERs than ENH_1. For the iris configurations enhancement does not improve the EERs. This is very likely caused by the block artefacts of the enhancement procedures which are carried to the polar CS-Images.

Considering the iris configurations the results show that the best EERs are reached using lg as feature extractor. Furthermore, the different variations for lg in terms of number of rows and row height (r / h_r) show that an increasing number of rows improves the verification performance. Overall configurations the best EERs are achieved using lg, hd(50,10) and lg, hd(64,08). Although lg, hd(50,10) ignores 12 pixel of each image the results are equal to the second configuration.

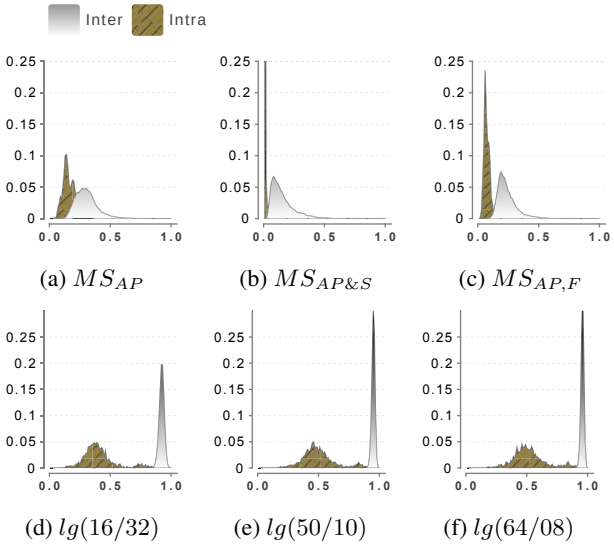

Figure 6: Intra-, Interclass SDs for selected configurations. [X-Axis: Matching Score, Y-Axis: Probability]

Regarding the two different polar-transformation formats, the results show that the larger format improves the EERs for the feature extractors which are assessed for both formats (lg and ko).

In Fig. 6 the intra-, interclass SDs for selected FP and iris configurations are depicted in the first and second row, respectively. These charts point out a significant difference which is not recognizable when considering just the EERs. Basically, they illustrate that the intra- and interclass SDs of the depicted FP and iris configurations are statistically significantly different.

For the FP configurations the charts for the three different matching procedures (ENH_{NO}) illustrate that by including shape information the separability is improved. Compared to the FP configurations, the interclass SDs of the iris configurations show a low variance and are thus narrow shaped. On the other hand, the intraclass SDs show a high variance and are broad shaped. Thereby, an increasing number of rows enforces this observation and the separability increases.

3.3. Identification Performance Evaluation

An overview on the identification performance is depicted in Fig. 7. For each configuration, the Rank 1 recognition rates are given for TS_1, TS_2 and for the combination of both (TS_1 & TS_2). Results show, that the recognition

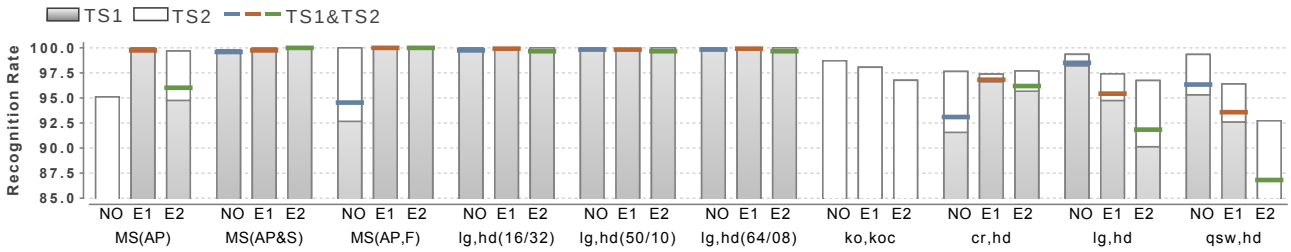

Figure 7: Identification performance evaluation - Rank 1 detection rates

rates for TS_1 are lower than for TS_2. The total recognition rate for the combination of TS_1 & TS_2 is somewhere in-between. The lower rates for TS_1 are caused by the higher degree of CS-variations in TS_1.

For the FP configurations each matching procedure achieves 100% recognition rate for at least one enhancement procedure. Surprisingly, nearly all iris configurations which use lg and 512×512 pixels achieve a recognition rate of 100% independent of the enhancement.

3.4. Intra-, Interclass Subset Analysis

In order to illustrate the impact of the testset structure and the enhancement procedures on the performance an analysis of the intra- and interclass SD subsets is presented.

For this purpose, the cumulative distribution functions (CDFs) of the intra- and interclass SDs of each testset are considered individually for MS_{AP} (without and with enhancement). The intraclass CDFs in Fig. 8a illustrate that

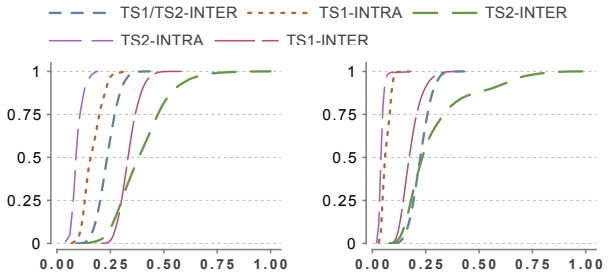

(a) $MS_{AP}/\ ENH_{NO}$ (b) $MS_{AP}/\ ENH_2$

Figure 8: CDFs for the intra-/ interclass SD subsets of two selected configurations. [X-Axis: Matching Score, Y-Axis: Probability]

the intraclass MSs of TS_1 are inferior than those from TS_2. Thereby, Fig. 8b shows that ENH_2 reduces this difference and the intraclass CDFs get closer and shift to the left. Although the interclass CDFs also shift slightly to the left the overlap between the intra- and interclass CDFs decreases and thus the performance is improved.

The inferior intraclass MSs of TS_1 are caused by CS variations included in TS_1. The CDFs for all intraclass SD subsets of TS_1 computed with $MS_{AP}/\ ENH_{NO}$ are shown in Fig. 9.

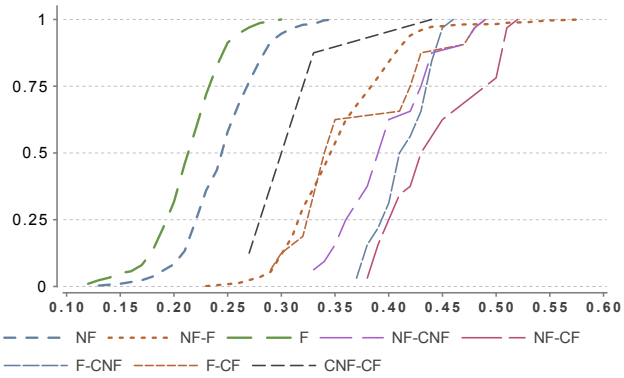

Figure 9: Intraclass SD Subset Analysis for TS_1. NF = No Flash, F = Flash, CNF = Cut No Flash, CF = Cut Flash. [X-Axis: Matching Score, Y-Axis: Probability]

As expected, the CS-Images captured with and without flash (F, NF) are quite similar to each other. Furthermore, CS-Images of CSs captured with flash (F) are more similar to each other than those captured without flash (NF). MSs computed between CS-Images captured without and those with flash (NF-F) show up inferior MSs. Finally, and as investigated in [15, 14] the chart illustrates the impact of cross-cutting the log end on the performance. Matching scores computed between the initial log end CS-Images and the cross-cut log end CS-Images are shown in the subsets: F-CF, F-CNF, NF-CF and NF-CNF. Fig. 9 illustrates that these subsets show inferior MSs compared to the other subsets.

4. Conclusions

This work demonstrates that FP and iris recognition based approaches can be successfully transferred to the field of wood log tracking. Based on the variety of 155 logs the results are a first indication for the applicability of log biometrics to log identification.

In case of the FP recognition based approach the best

results were achieved by including shape information in the matching procedure $MS_{AP,F}$. Furthermore, the results show that the performance of the FP configurations is significantly improved by the enhancement procedures. For the iris recognition based approaches the best results were achieved using lg features and hd as comparator. Thereby, a larger format and an increasing number of rows for the feature extraction is beneficial for the performance.

In the identification performance experiments the FP based approach and all iris configurations which use lg and 512×512 pixels achieve 100% detection rate at Rank 1. It can be concluded that Gabor features are well suited to extract discriminative annual ring pattern features.

Future research should deal with the impact of automated pith estimation and CS segmentation on the biometric system performance.

References

[1] W. Barrett. Biometrics of cut tree faces. In T. Sobh, editor, *Advances in Computer and Information Sciences and Engineering*, pages 562–565. Springer Netherlands, 2008.

[2] S. Chiorescu and A. Grönlund. The fingerprint approach: using data generated by a 2-axis log scanner to accomplish traceability in the sawmill's log yard. *Forest Products Journal*, 53:78–86, 2003.

[3] S. Chiorescu and A. Grönlund. The fingerprint method: Using over-bark and under-bark log measurement data generated by three-dimensional log scanners in combination with radiofrequency identification tags to achieve traceability in the log yard at the sawmill. *Scandinavian Journal of Forest Research*, 19(4):374–383, 2004.

[4] EuropeanParliament. Regulation (EU) No 995/2010 of the European Parliament and of the council of 20th October 2010 laying down the obligations of operators who place timber and timber products on the market, 2010.

[5] J. Flodin, J. Oja, and A. Grönlund. Fingerprint traceability of logs using the outer shape and the tracheid effect. *Forest Products Journal*, 58(4):21–27, 2008.

[6] L. Hong, Y. Wan, and A. Jain. Fingerprint image enhancement: Algorithm and performance evaluation. *IEEE Trans. Pattern Anal. Mach. Intell.*, 20(8):777–789, Aug. 1998.

[7] A. K. Jain, S. Prabhakar, L. Hong, and S. Pankanti. Filterbank-based fingerprint matching. *IEEE Transactions on Image Processing*, 9(5):846–859, May 2000.

[8] J.-G. Ko, Y.-H. Gil, J.-H. Yoo, and K.-I. Chung. A novel and efficient feature extraction method for iris recognition. *ETRI Journal*, 29(3):399 – 401, 2007.

[9] L. Ma, T. Tan, Y. Wang, and D. Zhang. Efficient iris recognition by characterizing key local variations. *IEEE Transactions on Image Processing*, 13:739–750, 2004.

[10] L. Masek. Recognition of Human Iris Patterns for Biometric Identification, Master's thesis, University of Western Australia, 2003.

[11] K. Norell and J. Lindblad. Spatially-variant morphological operations on binary images based on the polar distance transform. In *Proceedings of 19th International Conference on Pattern Recognition (ICPR'08)*, IEEE Proceedings. IEEE Computer Society, 2008.

[12] C. Rathgeb and A. Uhl. Secure iris recognition based on local intensity variations. In *Proceedings of the International Conference on Image Analysis and Recognition (ICIAR'10)*, volume 6112 of *Springer LNCS*, pages 266–275, Povoa de Varzim, Portugal, June 2010.

[13] C. Rathgeb, A. Uhl, and P. Wild. *Iris Recognition: From Segmentation to Template Security*, volume 59 of *Advances in Information Security*. Springer Verlag, 2013.

[14] R. Schraml, J. Charwat-Pessler, A. Petutschnigg, and A. Uhl. Robustness of biometric wood log traceability using digital log end images. Technical report, University of Salzburg, 2014.

[15] R. Schraml, J. Charwat-Pessler, and A. Uhl. Temporal and longitudinal variances in wood log cross-section image analysis. In *IEEE International Conference on Image Processing 2014 (ICIP 2014)*, Paris, FR, Oct. 2014.

[16] R. Schraml and A. Uhl. Pith estimation on rough log end images using local Fourier spectrum analysis. In *Proceedings of the 14th Conference on Computer Graphics and Imaging (CGIM'13)*, Innsbruck, AUT, Feb. 2013.

[17] R. Schraml and A. Uhl. Similarity based cross-section segmentation in rough log end images. In *Proceedings of the 10th Artificial Intelligence Applications and Innovations Conference(AIAI 2014)*, volume 436 of *IFIP Advances in Information and Communication Technology*, pages 614–621, Rhodes, GR, 2014. Springer Heidelberg Berline.

[18] R. Uusijärvi. Indisputable key project. `http://interop-vlab.eu/ei_public_deliverables/indisputable-key`, 2010. [last accessed: 28.07.2011].

[19] J. Wayman, A. Jain, and D. Maltoni. *Biometric Systems*. Springer Berlin / Heidelberg, 2005.